Ultrahigh-pressure disordered eight-coordinated phase of Mg_2GeO_4: Analogue for super-Earth mantles

Rajkrishna Dutta[a,b,1], **Sally June Tracy**[a], **R. E. Cohen**[a], **Francesca Miozzi**[a], **Kai Luo**[a], **Jing Yang**[a], **Pamela C. Burnley**[c], **Dean Smith**[d], **Yue Meng**[d], **Stella Chariton**[e], **Vitali B. Prakapenka**[e], **and Thomas S. Duffy**[b]

[a]Earth and Planets Laboratory, Carnegie Institution for Science, Washington, DC 20015; [b]Department of Geosciences, Princeton University, Princeton, NJ 08544; [c]Department of Geoscience, University of Nevada, Las Vegas, NV 89154; [d]High-Pressure Collaborative Access Team (HPCAT), X-Ray Science Division, Argonne National Laboratory, Argonne, IL 60439; and [e]Center for Advanced Radiation Sources, The University of Chicago, Chicago, IL 60637

Edited by David Kohlstedt, N. H. Winchell School of Earth Sciences, University of Minnesota, Minneapolis, MN; received August 5, 2021; accepted December 20, 2021

Mg_2GeO_4 is important as an analog for the ultrahigh-pressure behavior of Mg_2SiO_4, a major component of planetary interiors. In this study, we have investigated magnesium germanate to 275 GPa and over 2,000 K using a laser-heated diamond anvil cell combined with in situ synchrotron X-ray diffraction and density functional theory (DFT) computations. The experimental results are consistent with the formation of a phase with disordered Mg and Ge, in which germanium adopts eightfold coordination with oxygen: the cubic, Th_3P_4-type structure. DFT computations suggest partial Mg-Ge order, resulting in a tetragonal $I\bar{4}2d$ structure indistinguishable from $I\bar{4}3d$ Th_3P_4 in our experiments. If applicable to silicates, the formation of this highly coordinated and intrinsically disordered phase may have important implications for the interior mineralogy of large, rocky extrasolar planets.

post-postperovskite | super-Earth mineralogy | order–disorder transition

A large number of exoplanets have been discovered in recent years, including many planets whose mean densities indicate that they have rocky interiors that may be up to 10 times more massive than the Earth (1). There is interest in understanding the mineralogy of the deep interiors of such bodies where the pressure at the core–mantle boundary is predicted to reach up to 1 TPa (2–4). Theoretical calculations suggest that silicate structures with partial or complete eightfold coordination of silicon by oxygen can be stabilized above 500 GPa (4). These pressures are expected to be reached within the mantles of rocky exoplanets of ~4 Earth masses or greater (3, 4). Phase changes with accompanying changes in cation coordination number may strongly affect the structure, dynamics, and heat flow in exoplanet interiors (1, 5).

Germanates are known to be good analogs for silicates, as they undergo similar phase transitions, but at lower pressures (6, 7). For example, the perovskite (Pv) to postperovskite (pPv) transition occurs near 65 GPa in $MgGeO_3$ (8), compared with ~125 GPa in the corresponding silicate. Recently, a theoretical study examined ultrahigh-pressure transitions in the MgO-GeO_2 system and suggested that it can be an excellent analog system for ultrahigh-pressure phase transitions in silicate minerals (9). Those calculations predicted that $MgGeO_3$ pPv and MgO combine to form an eight-coordinated tetragonal phase of Mg_2GeO_4 ($I\bar{4}2d$) at ~175 GPa (9) (*SI Appendix*, Fig. S1). This transition pressure is experimentally accessible using a laser-heated diamond anvil cell. The same transition is predicted to occur at ~490 GPa (4) in the silicate, which is beyond the limit of conventional, static compression techniques.

Here, we report laser-heated diamond anvil cell experiments to pressures as high as 275 GPa and find that cubic, Th_3P_4-type ($I\bar{4}3d$), or partially disordered $I\bar{4}2d$ Mg_2GeO_4 is synthesized under such conditions. Our computations suggest a gradual disordering from an ordered $I\bar{4}2d$ structure to a partially disordered structure (experimentally indistinguishable from disordered $I\bar{4}3d$ structure) at high temperatures. Structures containing disordered ions of very different valences, Ge^{4+} and Mg^{2+}, are highly unusual but may occur in other high-pressure systems at high temperatures. The calculations also reveal the atomic structure and pressure–volume relationship of the disordered phase. The formation of the Th_3P_4-type *or* $I\bar{4}2d$ phase in the corresponding silicate at higher pressures would have important implications for the interior mineralogy of large, rocky extrasolar planets.

Results and Discussion

In a series of experiments (Table S1), Mg_2GeO_4 olivine samples were compressed to pressures between 115 and 275 GPa. Prior to any heating, the X-ray diffraction (XRD) patterns contained no sample diffraction peaks, indicating the germanate underwent pressure-induced amorphization at these conditions (10). Fig. 1 shows XRD patterns obtained on Mg_2GeO_4 samples that had been heated above 2,000 K at pressures between 161 and 275 GPa. A consistent set of new diffraction peaks is observed in all of these patterns. The ordered, tetragonal $I\bar{4}2d$ structure has been predicted by density functional theory (DFT) to be more stable than the dissociation products $MgGeO_3$ pPv + MgO in this pressure range (9). We carried out theoretical calculations to optimize this structure at pressures relevant to our experimental

Significance

This work presents experimental evidence for the formation of a phase with eightfold coordination of germanium by oxygen in Mg_2GeO_4, a well-known analogue of Mg_2SiO_4 at extreme pressure and temperatures. Using both experiments and theoretical computations, we have determined the structure, equation of state, and phase stability of this phase at pressures above 200 GPa. The existence of this phase in the silicate counterpart may play an important role in the structure and dynamics of the deep interiors of large, rocky exoplanets.

Author contributions: R.D., S.J.T., R.E.C., and T.S.D. designed research; R.D., R.E.C., F.M., K.L., J.Y., and T.S.D. performed research; P.C.B., D.S., Y.M., S.C., and V.B.P. contributed new reagents/analytic tools; R.D., S.J.T., and R.E.C. analyzed data; and R.D., R.E.C., and T.S.D. wrote the paper.

The authors declare no competing interest.

This article is a PNAS Direct Submission.

[1]To whom correspondence may be addressed. Email: rdutta@carnegiescience.edu.

This article contains supporting information online at http://www.pnas.org/lookup/suppl/doi:10.1073/pnas.2114424119/-/DCSupplemental.

Published February 14, 2022.

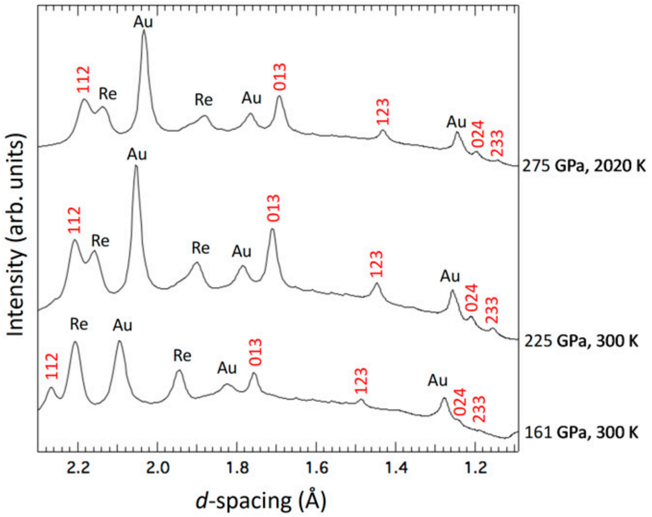

Fig. 1. XRD patterns of the Th_3P_4-type phase of Mg_2GeO_4 at 161, 225, and 275 GPa. The two lower pressure patterns are collected upon quench to 300 K after heating to 1,806 and 3,650 K, respectively, whereas the upper pattern was collected in situ at 2,020 K. Peaks from Th_3P_4-type Mg_2GeO_4 are indicated with Miller indices.

conditions. A comparison of the new peak positions observed in our experiments with those expected for the theoretically predicted $I\bar{4}2d$-type Mg_2GeO_4 phase show similarities in peak positions, but the expected splittings associated with the tetragonal phase are not observed (*SI Appendix*, Fig. S8). This is suggestive of formation instead of a related, higher-symmetry phase. Under the assumption that the unit cell of the new phase is cubic, only a single indexing is possible, consistent with a body-centered, cubic lattice ($h + k + l = 2n$). Within the minimal supergroups of $I\bar{4}2d$ (No. 122), space group $I\bar{4}3d$ (No. 220) provides the only possible solution. Of ∼40 candidate structure types for the AB_2X_4 stoichiometry (11), only one structure with this space group is known: the thorium phosphide structure, Th_3P_4 ($I\bar{4}3d$, Z = 4). Fitting the observed diffraction data to this structure yields a good match to the peak positions (Table S2).

The Th_3P_4-type Mg_2GeO_4 structure can be related to the tetragonal $I\bar{4}2d$ phase through an order–disorder transition (12). The ordered tetragonal structure has two cation sites, Mg (*8d*) and Ge (*4a*), and O occupies the *16e* site. The Th_3P_4 structure is intrinsically disordered, with both cations having partial occupancy of the *12a* Wyckoff site (Mg: 2/3 and Ge: 1/3), and O occupies the *16b* site. A phase-exhibiting cation disorder between Mg^{2+} and Ge^{4+} might be considered surprising, given the large difference in cation radius and valence. We first considered the relative stability of the ordered $I\bar{4}2d$ phase compared with the completely disordered, cubic $I\bar{4}3d$. The disordering enthalpy increases significantly with pressure (70 to 342 GPa): ΔH/fu = 0.37 to 1.10 eV, where fu = formula unit. Counteracting the enthalpy of disorder is the configurational entropy, which is zero in the completely ordered, tetragonal $I\bar{4}2d$ and $S/k_B/fu$ = 1.90954 for the cubic, disordered phase. The transition from completely ordered tetragonal to completely disordered cubic phase occurs when the Gibbs free energy difference $\Delta G = \Delta H - T\Delta S = 0$ (where S is the ideal, configurational entropy for each phase) thus ranges from 2,233 to 6,718 K for 70 to 342 GPa (*SI Appendix*, Fig. S7).

The ground state structure was predicted to be the ordered, tetragonal $I\bar{4}2d$ structure (12). However, our experiments are consistent with completely disordered, cubic $I\bar{4}3d$ structure. The explanation may lie in growth and ordering kinetics. The disordered phase may form during crystal growth from the starting materials and then not be able to order on the time scale of the experiments. Highly charged ions are expected to diffuse and order slowly. Similar behavior is seen in many systems. For example, lead magnesium niobate ($PbMg_{1/3}Nb_{2/3}O_3$) is typically observed as optically isotropic and cubic in XRD, because the highly charged Nb^{5+} diffuses slowly to order with Mg^{2+} to form the ordered structure predicted by theory (14). However, ordering in that case could be observed with transmission electron microscopy (15).

The XRD pattern obtained from a sample heated at 240 GPa and quenched to room temperature (run H3_2) shows peaks from the Th_3P_4-type Mg_2GeO_4 phase (Fig. 2*A* and *SI Appendix*, Fig. S9). To examine these results, we generated a set of special quasirandom structures (SQS) using the ATAT toolkit (16), which generates supercells that resemble a partially or completely disordered structures (224-atom supercell with 32 Ge atoms and 64 Mg atoms in our case). The resulting structures were then optimized using Quantum Espresso (17). The average structure was obtained using FINDSYM (18). The computed, structural parameters were used as an initial model to carry out a Rietveld refinement (Fig. 2*A*) of the quenched diffraction pattern. The corresponding two-dimensional diffraction image (*SI Appendix*, Fig. S10) shows smooth diffraction rings, suggesting minimal preferred orientation. In an experiment at 187 GPa (run H4), we attempted to decrease the laser power in small steps to replicate slow cooling of the Th_3P_4-type phase (3,032 to 300 K in ∼14 min). The ordered $I\bar{4}2d$ phase was still not observed. Further work will be necessary to better determine if the completely or highly ordered $I\bar{4}2d$ phase can be synthesized/observed at lower temperatures.

Although many minerals and alloys have sharp, first-order or fairly sharp continuous transitions from nearly ordered to disordered structures, it is also possible to have other behaviors, including smooth disordering with temperature, depending on the behavior of $H(Q)$ compared with $S(Q)$ (13), where Q is the order parameter. The tetragonal structure can be partly disordered, with an order parameter, Q, varying from 0 for the disordered $I\bar{4}3d$ structure to 1 for the completely ordered $I\bar{4}2d$ phase. The relationship is the following: X_{Mg} (8d) = $Q \times 1/3 + 2/3$ and X_{Mg} (4a) = $-Q \times 2/3 + 2/3$. This is known as convergent ordering because the sites become equivalent when completely disordered. Our DFT computations show a gradual disordering with temperature within the tetragonal phase with no abrupt phase transition. A recent computational study (12) claims a phase transition from a completely ordered to a completely disordered structure. However, their figure 5 shows that the phase remains partially ordered at temperatures higher than their suggested transition temperature, which they based on a peak in the heat capacity. Thus, their computations are actually consistent with ours and show that a completely disordered structure does not form even at extremely high temperatures (∼10,000 K).

Fig. 3*A* summarizes the variation in order parameter, Q, with temperature at 150, 200, and 300 GPa. The *c/a* ratio increases with ordering, from 1 in the cubic phase to 1.025 to 1.038 in fully ordered tetragonal (Fig. 3*B*). At 200 GPa, we estimate Q < ∼0.53 cannot be distinguished experimentally in our experiments. As an example, we have shown calculated diffraction patterns for $Q = 0.25$ and $Q = 0$, with c/a strain less than 1% along with the observed pattern at 187 GPa. They are experimentally indistinguishable (Fig. 3*C*). The diffraction patterns throughout the manuscript have therefore been indexed with the $Q = 0$ cubic $I\bar{4}3d$ Th_3P_4 structure (Fig. 2*B*), and experimental results are referred to as the Th_3P_4-type phase for simplicity. Further details of the Th_3P_4-type structure are provided in the *SI Appendix*. However, the diffraction splittings from strains of 2 to 4% computed for Q = 0.8 to 1 are never observed.

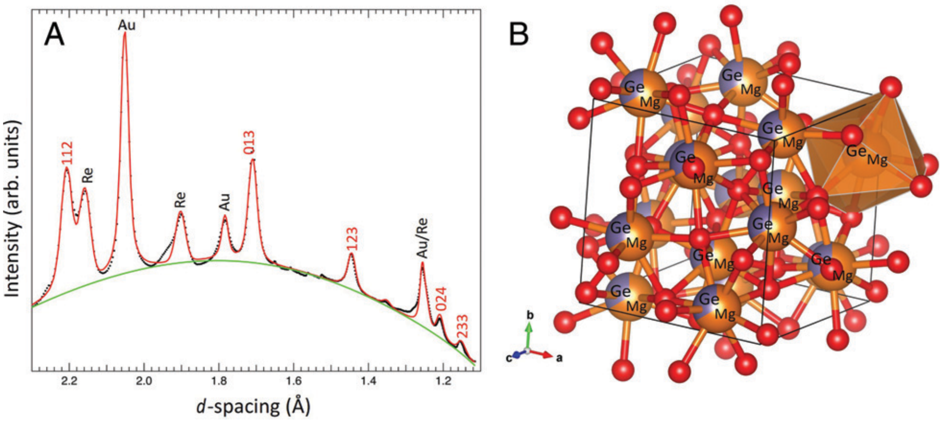

Fig. 2. (*A*) Rietveld refinement of the XRD pattern (black) obtained after heating Mg_2GeO_4 to 3,650 K at 240 GPa, with subsequent quenching to room temperature [a = 5.4055 (2) Å; oxygen coordinate, O_x = 0.0468]. Red and green curves show the fit and background, respectively. Miller indices of the Th_3P_4-type Mg_2GeO_4 are shown above the observed diffraction pattern. A small amount of untransformed starting material is present near 1.95 Å. (*B*) Structure of the Th_3P_4-type phase: Red spheres are oxygen atoms, and orange/mauve spheres represent the Mg/Ge site, with shading to indicate two-third occupancy by Mg and one-third occupancy by Ge. A representative $(Mg,Ge)O_8$ polyhedron is also shown.

The lattice parameters and atomic positions obtained from the experiments and computations are in good agreement with each other (Table S3). The unit cell dimension obtained from the Rietveld refinement of the experimental data at 184 GPa is 5.4930 Å, and the calculations yield 5.492 Å at 193 GPa. If the O is placed at the ideal x value for the Th_3P_4 structure ($x = 1/12$), the Mg–O and Ge–O bond lengths would be 1.903 and 1.898 Å.

The Mg–O and Ge–O bond lengths from the experiments (theory) are 2.080 (2.015 Å) and 1.745 Å (1.796 Å). Our results indicate that the structure can be stabilized for x = 0.055 (0.0646), far from the ideal value. The Ge–O bond length of the Th_3P_4-type phase is increased by a few percent relative to that in $MgGeO_3$ pPv structure (Ge–O: 1.70 Å) at 184 GPa (19), consistent with an increase in coordination relative to the lower-pressure phase assemblage.

The pressure–temperature conditions achieved in our experiments are shown in Fig. 4. For our lowest pressure experiment (115 GPa), the diffraction peaks obtained during heating (*SI Appendix*, Fig. S11) can be assigned to $MgGeO_3$ pPv (*Cmcm*) and B1-MgO ($Fm\bar{3}m$), indicating that the starting material has decomposed into this assemblage upon heating. These results are consistent with theoretical predictions at this pressure (*SI Appendix*, Fig. S11). It is also notable that prolonged heating near 2,000 K was required at this pressure to produce any diffraction peaks at all, suggesting that the decomposition of pressure-amorphized Mg_2GeO_4 into pPv and periclase (MgO) may be kinetically slow because of the atomic diffusion required for the decomposition reaction.

For experiments between 130 and 170 GPa, the results are more complicated. The diffraction data are consistent with the Th_3P_4-type phase upon initial heating of the amorphous sample. However, upon prolonged heating and/or at higher temperatures, peaks of the pPv phase emerge and grow at the expense of Th_3P_4-type peaks (Run G3; Fig. 4*B*). Additional results for the pPv phase are shown in *SI Appendix*, Fig. S12 and Table S4. In the higher-pressure runs above 175 GPa, peaks consistent with the Th_3P_4-type phase are observed to form and/or grow during heating in all experiments. For example, in one run (H2_2), the pPv phase was synthesized at lower pressures, and then, the pressure in the cell was increased to 175 GPa. Upon heating at this pressure, the pPv peaks diminish over time while Th_3P_4-type peaks grow (Fig. 4*C*). Complete transformations from Mg_2GeO_4 to $MgGeO_3$ + MgO and vice versa are not observed because of the slow reaction kinetics. In run H4, a fresh sample was heated at 187 GPa, and only Th_3P_4-type peaks were observed within ∼2 min of laser heating and retained even after prolonged heating to 3,000 K.

These observations indicate that below 175 GPa, the Th_3P_4-type Mg_2GeO_4 phase is likely a metastable phase formed on initial heating in this pressure range. The metastable behavior can be understood as a result of transformation kinetics of the highly coordinated, amorphous phase that forms on room temperature compression. Experiments on GeO_2 glass show that the Ge–O coordination number increases with compression (20). Thus, we expect the unheated Mg_2GeO_4 material to be a dense, highly coordinated glass. Therefore, on initial heating at lower temperatures, it may be kinetically easier to transform to the cation-disordered, eightfold-coordinated phase of Mg_2GeO_4 rather than decompose into the pPv phase and MgO. Similar behavior has been observed in experiments on the SiO_2 polymorph cristobalite, in which seifertite, a phase that is thermodynamically stable at pressures above 100 GPa, was observed to form metastably on heating at pressures as low as ∼11 GPa within the stability field of stishovite (21). This was interpreted as a result of the faster kinetics for the formation of metastable seifertite from the cristobalite X-I phase. Upon prolonged heating to higher temperatures, seifertite eventually transformed into the thermodynamically stable stishovite structure, similar to the behavior we observe here.

Fig. 5*A* shows the pressure–volume relation of the Th_3P_4-type Mg_2GeO_4 phase at 300 K (0 K for theory). No pressure-transmitting medium was used in these experiments to maximize the sample volume at extreme pressures. To minimize the effect of differential stresses on the experimental results, we have included only data points obtained immediately after quenching from high temperature at each pressure step. Theoretical calculations were also performed to test the reliability of the equation of state parameters. A third-order Birch–Murnaghan fit (solid: experiments and dashed: theory) to the data yields V_0 = 252.5 (3.2) $Å^3$, K_{0T} = 188 (11) GPa and V_0 = 261.6 (1.2) $Å^3$, and K_{0T} = 170 (3) GPa, respectively; K'_{0T} was fixed at 4 in both cases. The ambient pressure bulk modulus is comparable to that of the pPv $MgGeO_3$ phase (K_{0T} = 192 (5) GPa, $K'_{0T} = 4$).

Fig. 5*B* compares the densities of phases in the $MgO–GeO_2$ system (19, 22–27). The densities of $MgGeO_3$ + MgO mixtures were calculated assuming an ideal solid solution (i.e., the molar volumes are additive). The density of the mixture (ρ) is given by the following:

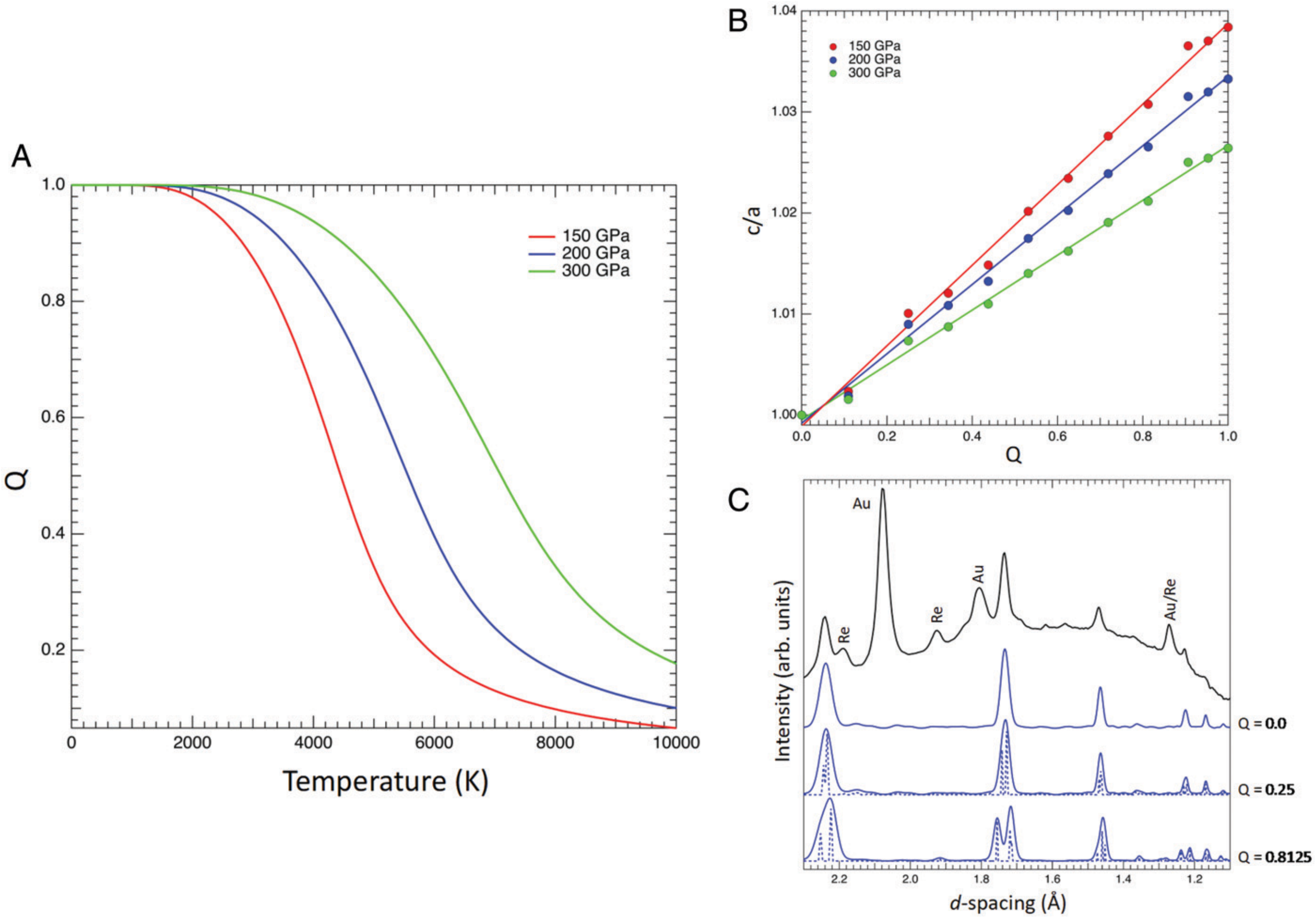

Fig. 3. (*A*) Variation of order parameter, *Q*, with temperature for $I\bar{4}2d$ Mg_2GeO_4 from DFT calculations at 150 (red), 200 (blue), and 300 (green) GPa. $Q = 1$ corresponds to a fully ordered structure. (*B*) Variation in *c/a* with order parameter at the same pressures. (*C*) Comparison of a representative observed XRD pattern (black) at 187 GPa and 2,010 K with the theoretically calculated structures (224 atom supercell) with Q = 0.8125, Q = 0.25, and Q = 0 at 200 GPa. Dashed and solid blue lines represent the simulated patterns with delta and pseudo-Voigt peak functions, respectively. The full width at half maximum of the observed sample peaks (0.1473 Å) has been used as Gaussian broadening for the simulated patterns for the latter.

$$\frac{1}{\rho(P,T)} = \frac{(1-m_2)}{\rho_1(P,T)} + \frac{m_2}{\rho_2(P,T)},$$

where m and ρ are the mass fraction and density of the individual components (labeled as 1 and 2). Our results indicate that the transition from pPv and MgO to the Th_3P_4-type phase produces a substantial (2.4%) change in density at 190 GPa.

Conclusions

We have shown that Mg_2GeO_4 adopts the thorium phosphide or a highly disordered, tetragonal $I\bar{4}2d$ structure at pressures above ~175 GPa. The phase is calculated to be ~2.4% denser than the mixture of $MgGeO_3$ pPv and MgO. This describes an experimental synthesis of a phase with Ge in eightfold coordination, with oxygen and an occurrence of the Th_3P_4-type phase in an oxide. Just as the discovery of widespread, six-coordinated germanates/silicates profoundly altered our understanding of silicate crystal chemistry and its role in the Earth's deep interior, the discovery of an eightfold-coordinated, intrinsically disordered germanate opens the possibility of previously unexplored crystal–chemical behavior in the silicate minerals of large, rocky exoplanets. Our results also raise the possibility that this structure or the related $I\bar{4}2d$ structure could also be adopted by other oxide minerals at extreme pressures. Thus, our results suggest the possibility of interesting crystal chemistry in A_3O_4- and AB_2O_4-type compounds that warrant further exploration.

Changes in silicon coordination in minerals can influence the structure and dynamics of planetary interiors (28). The transition in silicates from tetrahedral (fourfold) to octahedral (sixfold) coordination of silicon by oxygen occurring near 660-km depth defines the major structural boundary in Earth's mantle (29). In the Earth, six-coordinated silicate phases are expected to be stable throughout the lower mantle with $(Mg,Fe)SiO_3$ pPv and SiO_2 seifertite (α-PbO_2–type) stable at core–mantle boundary conditions (~135 GPa). In the case of SiO_2, a further transition to the $Pa\bar{3}$ type is observed at 268 GPa (30), but this phase retains sixfold coordination (sometimes described as 6 + 2). Increases in coordination above six have been reported in SiO_2 glass at ultrahigh pressures (31). However, as far as we are aware, there is no experimental evidence for silicon coordination greater than six in any high-pressure crystalline silicates or their analogs.

pPv $(Mg,Fe)SiO_3$ is the expected silicate phase at the base of Earth's mantle, but post-pPv phases with Si–O coordination >6 may play a decisive role in terrestrial super-Earths of four or greater Earth masses (*SI Appendix*, Fig. S1). If the Th_3P_4-type or the closely related, partially disordered $I\bar{4}2d$ phase also exists in Mg_2SiO_4, the change in coordination from sixfold to eightfold may be accompanied by major changes in physical, chemical, and thermodynamic properties. The ~2.4% volume change associated with the transition is large (Δρ = ~1.5% for Pv to pPv) for ultrahigh-pressure phase transitions and may affect the dynamic

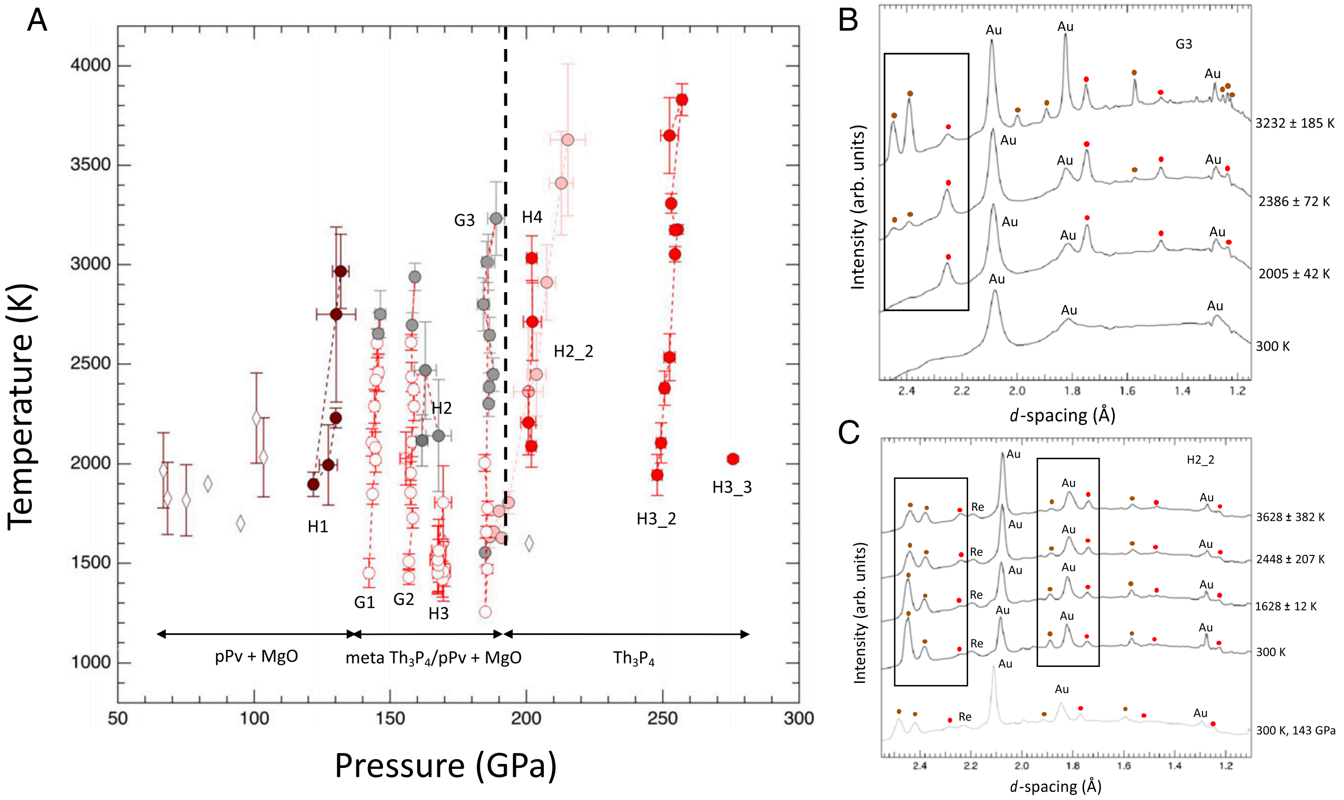

Fig. 4. (*A*) Phase diagram of Mg_2GeO_4. Solid brown circles indicate P-T conditions in which only $MgGeO_3$ pPv + MgO is observed. The solid red circles show P-T conditions in which diffraction patterns showed only Th_3P_4-type Mg_2GeO_4. The open red circles show lower-temperature conditions at which Th_3P_4-type phase is observed but is interpreted as metastable. The solid gray symbols indicate conditions at which diffraction from both pPv and Th_3P_4 are observed, but the pPv peaks grow and the Th_3P_4 peaks diminish with increasing heating time and/or temperature. The growth of pPv at the expense of Th_3P_4 is taken as evidence that pPv is the stable phase at these conditions. Conversely, the solid pink symbols show conditions at which the peaks of the Th_3P_4 phase are observed to grow, and the pPv peaks diminish with heating time and/or temperature. This is evidence that the Th_3P_4 phase is stable at these conditions. The black line is the estimated phase boundary for the pPv + $MgO \rightarrow Th_3P_4$-type Mg_2GeO_4. Open brown diamonds are P-T points at which pPv was observed in previous work (19). The stability regions for pPv+MgO, pPv + MgO with metastable Th_3P_4 at lower temperatures, and Th_3P_4 are indicated at the bottom. (*B*) Diffraction patterns during a heating cycle at 169 GPa showing the growth of pPv peaks (brown circles) at the expense of Th_3P_4 peaks (red circles). (*C*) Diffraction patterns during a heating cycle at 175 GPa showing the growth of Th_3P_4-type phase (indicated by red circles) and decreased intensity of the pPv phase (indicated by brown circles).

behavior of the deep mantle. The intrinsically disordered nature of this phase may be an important feature as it suggests enhanced miscibility of chemical components at ultrahigh–pressure and temperature (P-T) conditions. Among chalcogenides, Th_3P_4-type phases are noted for their flexible structure and prevalence of defects, impurities, and disorder (32). This structural flexibility can affect rheology and transport properties. Compared with other structures, enhanced phonon scattering in this disordered phase may yield an anomalously low, thermal conductivity (33).

Materials and Methods

Experimental Procedure. Mg_2GeO_4 olivine samples were synthesized according to established procedures (23, 34) and confirmed by XRD. The sample was mixed with 10 weight % gold, which acted as a pressure calibrant and laser absorber. Rhenium gaskets were preindented, and ∼20-μm diameter holes were laser drilled to form the sample chamber in a diamond anvil cell. The sample + Au pellets were then loaded into a cell with beveled 50-μm culet anvils.

Angle-dispersive XRD was carried out at beamlines 13-ID-D and 16-ID-B of the Advanced Photon Source (APS) using monochromatic X-rays (λ = 0.3344 and 0.4066 Å, respectively) focused to dimensions of $3 \times 3\ \mu m^2$ and $5 \times 3\ \mu m^2$, respectively. CdTe or Si 1-M Pilatus detectors were used to collect the diffraction patterns. LaB_6 and CeO_2 standards were used to calibrate the detector position and orientation.

High temperatures were attained by double-sided heating with diode-pumped fiber lasers with ∼10 to 15 μm spot sizes. Temperature was increased in a stepwise fashion with ∼150 to 200 K steps and a heating duration of 1.5 to 2 min at each step (total heating duration: 7 to 26 min). The laser power was adjusted independently on both sides to keep temperature differences to <150 K. Temperatures were measured using spectroradiometry. Pressure was determined using the (111) reflection of Au (35). Thermal pressures were accounted for using the Mie–Grüneisen equation of state.

The two-dimensional XRD images were integrated to one-dimensional patterns using DIOPTAS (36) and fit using background-subtracted Voigt line shapes. Lattice parameters were calculated by least-squares refinement of the peak positions (37) or whole-profile Le Bail refinement as implemented in MAUD (38). For the whole-pattern refinement, the background was fit with a fourth-order polynomial; instrumental profile terms were fit with Gaussian Cagliotti terms. Sample-broadening incorporated isotrophic size and strain broadening.

Computational Details. We performed first-principles DFT calculations to determine the structural parameters of the $I\bar{4}2d$ and Th_3P_4-type Mg_2GeO_4 phases, constrain the equation of state over the range from 135 to 342 GPa, and examine the order–disorder transition. We used the QUANTUM ESPRESSO (17) plane wave pseudopotential code PWSCF to perform DFT computations with Perdew-Burke-Ernzerhof exchange correlation and GBRV (Garrity, Benett, Rabe and Vanderbilt) potentials (39) with a 4 × 4 × 4 Monkhorst–Pack *k*-point mesh in the supercell and an energy cutoff for the wavefunctions of 1,361 eV.

We simulated the disordered system using the special quasirandom structure method (40, 41), as implemented in the ATAT toolkit (16). We generated a 224-atom supercell and used the Monte Carlo method to find the most random structure considering clusters up to 2-cation pairs up to 5.0 Å for a tetragonal lattice. We constrained the supercell to be doubled in each direction of the cubic cell (i.e., 10.984 × 10.984 × 10.990 Å for our starting system. We

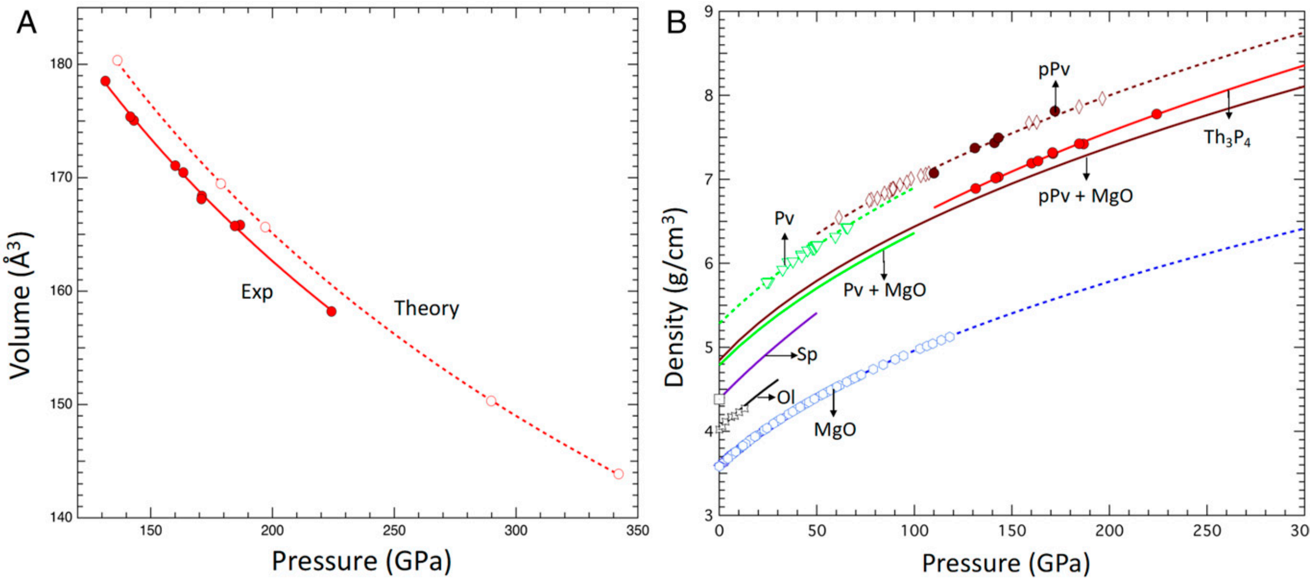

Fig. 5. (*A*) Equation of state of the Th_3P_4-type phase from experiments (300 K, solid red circles) and theoretical calculations (0 K, open red circles). Lines are third-order Birch–Murnaghan equation fits. (*B*) Densities of selected phases in the MgO-GeO_2 system. Solid circles are from this work (brown: pPv and red: Th_3P_4). Previous studies are indicated by open symbols: brown diamonds, pPv (19); green triangles, Pv (22); purple square, spinel (23, 24); black stars, olivine (25); and blue hexagons, B1-MgO (26, 27). The brown and green solid lines are the calculated densities of mixtures of $MgGeO_3$ Pv and pPv with MgO.

considered a set of SQS structures for $I\bar{4}2d$-type Mg_2GeO_4 for 13 different order parameters from $Q = 0$ to 1 (e.g., *SI Appendix*, Fig. S2). *H(Q)* fits well to a second-order polynomial, and higher-order fits were not justified (*SI Appendix*, Fig. S3). To test the convergence of our computations, SQS for clusters up to third, fourth, and sixth neighbors have also been explored (*SI Appendix*, Fig. S4). The resulting variation in volume with *Q* is shown in *SI Appendix*, Fig. S5.

We estimated the thermal pressure by performing first-principles molecular dynamics (MD) on the 224-atom supercell at 5,000 K for $a = 5.492$ Å. We performed constant number, volume and temperature (MD with the stochastic velocity rescaling (SVR) stochastic thermostat (50 fs timescale) and a time step about 1 fs (42). The run was 5 ps, with the first ps removed for equilibration. We obtained a pressure of 240.2 ± 0.2 GPa at 5,067 ± 11 K (nominal target T 5,000 K is used in all analyses here). Running a static relaxation using the same conditions gives $P = 195.6$ GPa, giving a thermal pressure of 44.6 GPa at 5,000 K. The MD pressures for cubic and tetragonal at 5,000 K are 240.2 and 241.8 GPa, respectively, showing that the thermal pressure does not depend strongly on the state of order.

We used the Γ-point and the same setup as for the MD computations above and performed static relaxations at pressures of 150, 200, and 300 GPa for each of the 13 *Q* values. A test run with denser *k*-point grid ($2 \times 2 \times 2$) did not yield significant differences in enthalpy (*SI Appendix*, Fig. S4). The entropy is given by $\frac{S}{k_B} = \sum X \ln X$, where the sum is over the sites, and *X* is the mole fraction of Mg or Ge on each site (*SI Appendix*, Fig. S6). The free energy is minimized at each temperature, giving the order parameter versus temperature.

Within DFT, we relaxed the ordered structures with respect to lattice parameters and atomic positions by optimizing the enthalpy at the same pressures that was determined for the SQS models of the cubic structure, giving seven points with pressures ranging from 70 to 342 GPa. A sample input file for $Q = 0.25$ has been provided with the *SI Appendix* (DOI: 10.17605/OSF.IO/FM87E).

Data Availability. A sample input file for the DFT calculations performed in this work has been deposited in the Open Science Framework (DOI: 10.17605/OSF.IO/FM87E). All other data are included in the article and/or the *SI Appendix*.

ACKNOWLEDGMENTS. We acknowledge helpful discussions with Michael Walter. We are also grateful to Peng Ni for his assistance with staring sample synthesis. This research was supported by the NSF—Earth Sciences (EAR-1836852). R.D. is grateful for support from the Carnegie Endowment. We acknowledge the support of GeoSoilEnviroCARS (Sector 13), which is supported by the NSF—Earth Sciences (EAR-1634415) and the US Department of Energy (DOE), Geosciences (DE-FG02-94ER14466). Portions of this work were performed at HPCAT (Sector 16), APS, Argonne National Laboratory. HPCAT operations are supported by DOE-National Nuclear Security Administration Office of Experimental Sciences. This research used resources of the APS, a DOE Office of Science User Facility operated by Argonne National Laboratory under Contract No. DE-AC02-06CH11357. R.E.C. gratefully acknowledges the Gauss Centre for Supercomputing e.V. (https://www.gauss-centre.eu/) for funding this project by providing computing time on the GCS Supercomputer SuperMUC-NG at Leibniz Supercomputing Centre (LRZ, http://www.lrz.de).

1. T. V. Hoolst, L. Noack, A. Rivoldini, Exoplanet interiors and habitability. *Adv. Phys. X* **4**, 1630316 (2019).
2. K. Umemoto, R. M. Wentzcovitch, Two-stage dissociation in $MgSiO_3$ post-perovskite. *Earth Planet. Sci. Lett.* **311**, 225–229 (2011).
3. T. S. Duffy, N. Madhusudhan, K. K. M. Lee, “Mineralogy of super-Earth planets” in *Treatise on Geophysics*, G. Schubert, Ed. (Elsevier, ed. 2, 2015), pp. 149–178.
4. K. Umemoto *et al.*, Phase transitions in $MgSiO_3$ post-perovskite in super-Earth mantles. *Earth Planet. Sci. Lett.* **478**, 40–45 (2017).
5. M. H. Shahnas, R. N. Pysklywec, D. A. Yuen, Penetrative convection in super-Earth planets: Consequences of $MgSiO_3$ postperovskite dissociation transition and implications for super-earth GJ876d. *J. Geophys. Res. Planets* **123**, 2162–2177 (2018).
6. A. E. Ringwood, M. Seabrook, High-pressure phase transformations in germanate pyroxenes and related compounds. *J. Geophys. Res.* **68**, 4601–4609 (1963).
7. C. V. Stan, R. Dutta, R. J. Cava, V. B. Prakapenka, T. S. Duffy, High-pressure study of perovskites and postperovskites in the (Mg, Fe)GeO_3 system. *Inorg. Chem.* **56**, 8026–8035 (2017).
8. K. Hirose, K. Kawamura, Y. Ohishi, S. Tateno, N. Sata, Stability and equation of state of $MgGeO_3$ post-perovskite phase. *Am. Min* **90**, 262–265 (2005).
9. K. Umemoto, R. M. Wentzcovitch, Ab initio exploration of post-PPV transitions in low-pressure analogs of $MgSiO_3$. *Phys. Rev. Mater.* **3**, 123601 (2019).
10. T. Nagai, K. Yano, M. Dejima, T. Yamanaka, Pressure-induced amorphization of Mg_2GeO_4-olivine. *Miner. J. Japan* **17**, 151–157 (1994).
11. X. Zhang, V. Stevanović, M. d’Avezac, S. Lany, A. Zunger, Prediction of A_2BX_4 metal-chalcogenide compounds via first-principles thermodynamics. *Phys. Rev. B Condens. Matter Mater. Phys.* **86**, 014109 (2012).
12. K. Umemoto, R. M. Wentzcovitch, Ab initio prediction of an order-disorder transition in Mg_2GeO_4: Implication for the nature of super-Earth’s mantles. *Phys. Rev. Mater.* **5**, 093604 (2021).
13. T. Holland, R. Powell, Thermodynamics of order-disorder in minerals; I, Symmetric formalism applied to minerals of fixed composition. *Am. Min.* **81**, 1413–1424 (1996).
14. N. Choudhury, Z. Wu, E. J. Walter, R. E. Cohen, Ab initio linear response and frozen phonons for the relaxor $PbMg_{1/3}Nb_{2/3}O_3$. *Phys. Rev. B Condens. Matter Mater. Phys.* **71**, 125134 (2005).

15. D. Fu *et al.*, Relaxor Pb(Mg$_{(1/3)}$Nb$_{(2/3))}$O$_3$: A ferroelectric with multiple inhomogeneities. *Phys. Rev. Lett.* **103**, 207601 (2009).
16. A. van de Walle *et al.*, Efficient stochastic generation of special quasirandom structures. *Calphad* **42**, 13–18 (2013).
17. P. Giannozzi *et al.*, QUANTUM ESPRESSO: A modular and open-source software project for quantum simulations of materials. *J. Phys. Condens. Matter* **21**, 395502 (2009).
18. H. T. Stokes, D. M. Hatch, FINDSYM: Program for identifying the space-group symmetry of a crystal. *J. Appl. Cryst.* **38**, 237–238 (2005).
19. A. Kubo *et al.*, Stability and equation of state of the post-perovskite phase in MgGeO$_3$ to 2 Mbar. *Geophys. Res. Lett.* **33**, L12S12 (2006).
20. Y. Kono *et al.*, Ultrahigh-pressure polyamorphism in GeO$_2$ glass with coordination number >6. *Proc. Natl. Acad. Sci. U.S.A.* **113**, 3436–3441 (2016).
21. T. Kubo, T. Kato, Y. Higo, K.-I Funakoshi, Curious kinetic behavior in silica polymorphs solves seifertite puzzle in shocked meteorite. *Sci. Adv.* **1**, e1500075 (2015).
22. C. E. Runge *et al.*, Equation of state of MgGeO$_3$ perovskite to 65 GPa: Comparison with the post-perovskite phase. *Phys. Chem. Miner.* **33**, 699–709 (2006).
23. R. B. Von Dreele, A. Navrotsky, A. L. Bowman, Refinement of the crystal structure of Mg$_2$GeO$_4$ spinel. *Acta Crystallogr. B* **33**, 2287–2288 (1977).
24. M. Blanchard, K. Wright, J. D. Gale, Atomistic simulation of Mg$_2$SiO$_4$ and Mg$_2$GeO$_4$ spinels: A new model. *Phys. Chem. Miner.* **32**, 332–338 (2005).
25. P. E. Petit, F. Guyot, G. Fiquet, J. P. Itié, High-pressure behaviour of germanate olivines studied by X-ray diffraction and X-ray absorption spectroscopy. *Phys. Chem. Miner.* **23**, 173–185 (1996).
26. S. Speziale, C.-S. Zha, T. S. Duffy, R. J. Hemley, H.-k Mao, Quasi-hydrostatic compression of magnesium oxide to 52 GPa: Implications for the pressure-volume-temperature equation of state. *J. Geophys. Res. Solid Earth* **106**, 515–528 (2001).
27. S. D. Jacobsen *et al.*, Compression of single-crystal magnesium oxide to 118 GPa and a ruby pressure gauge for helium pressure media. *Am. Min* **93**, 1823–1828 (2008).
28. A. P. van den Berg, D. A. Yuen, K. Umemoto, M. H. G. Jacobs, R. M. Wentzcovitch, Mass-dependent dynamics of terrestrial exoplanets using ab initio mineral properties. *Icarus* **317,** 412–426 (2019).
29. T. Irifune, A. Ringwood, Phase transformations in subducted oceanic-crust and buoyancy relationships at depths of 600-800 km in the mantle. *Earth Planet. Sci. Lett.* **117**, 101–110 (1993).
30. Y. Kuwayama, K. Hirose, N. Sata, Y. Ohishi, The pyrite-type high-pressure form of silica. *Science* **309**, 923–925 (2005).
31. C. Prescher *et al.*, Beyond sixfold coordinated Si in SiO$_2$ glass at ultrahigh pressures. *Proc. Natl. Acad. Sci. U.S.A.* **114**, 10041–10046 (2017).
32. C. E. Whiting, E. S. Vasquez, C. D. Barklay, "Uranium based materials as potential thermoelectric couples for future radioisotope power systems" in 2018 IEEE Aerospace Conference (2018), pp. 1–9.
33. G. J. Snyder, E. S. Toberer, "Complex thermoelectric materials" in *Materials for Sustainable Energy* (Macmillan Publishers Ltd, UK, 2010), pp. 101–110.
34. P. C. Burnley, "The effect of nonhydrostatic stress on the olivine-spinel transformation in Mg2GeO4," PhD thesis, University of California-Davis (1990).
35. Y. Fei *et al.*, Toward an internally consistent pressure scale. *Proc. Natl. Acad. Sci. U.S.A.* **104**, 9182–9186 (2007).
36. C. Prescher, V. B. Prakapenka, DIOPTAS: A program for reduction of two-dimensional X-ray diffraction data and data exploration. *High Press. Res.* **35**, 223–230 (2015).
37. T. J. B. Holland, S. A. T. Redfern, Unit cell refinement from powder diffraction data: The use of regression diagnostics. *Mineral. Mag.* **61**, 65–77 (1997).
38. L. Lutterotti, Total pattern fitting for the combined size–strain–stress–texture determination in thin film diffraction. *Nucl. Instrum. Methods Phys. Res. B* **268**, 334–340 (2010).
39. K. F. Garrity, J. W. Bennett, K. M. Rabe, D. Vanderbilt, Pseudopotentials for high-throughput DFT calculations. *Comput. Mater. Sci.* **81**, 446–452 (2014).
40. S. Wei, L. G. Ferreira, J. E. Bernard, A. Zunger, Electronic properties of random alloys: Special quasirandom structures. *Phys. Rev. B Condens. Matter* **42**, 9622–9649 (1990).
41. A. Zunger, S. Wei, L. G. Ferreira, J. E. Bernard, Special quasirandom structures. *Phys. Rev. Lett.* **65**, 353–356 (1990).
42. G. Bussi, D. Donadio, M. Parrinello, Canonical sampling through velocity rescaling. *J. Chem. Phys.* **126**, 014101 (2007).